



# Temperature influence on water transport in hardened cement pastes

Emeline Drouet, Stéphane Poyet, Jean-Michel Torrenti

## ► To cite this version:

Emeline Drouet, Stéphane Poyet, Jean-Michel Torrenti. Temperature influence on water transport in hardened cement pastes. *Cement and Concrete Research*, Elsevier, 2015, 76, pp.37-50. <10.1016/j.cemconres.2015.05.002>. <cea-01272801>

**HAL Id: cea-01272801**

**<https://hal-cea.archives-ouvertes.fr/cea-01272801>**

Submitted on 11 Feb 2016

**HAL** is a multi-disciplinary open access archive for the deposit and dissemination of scientific research documents, whether they are published or not. The documents may come from teaching and research institutions in France or abroad, or from public or private research centers.

L'archive ouverte pluridisciplinaire **HAL**, est destinée au dépôt et à la diffusion de documents scientifiques de niveau recherche, publiés ou non, émanant des établissements d'enseignement et de recherche français ou étrangers, des laboratoires publics ou privés.

# Temperature influence on water transport in hardened cement pastes.

---

Emeline DROUET <sup>a</sup>, Stéphane POYET <sup>a,\*</sup>, Jean-Michel TORRENTI <sup>b</sup>

<sup>a</sup> CEA, DEN, DPC, SECR, Laboratoire d'Etude du Comportement des Bétons et des Argiles, F-91191 Gif sur Yvette Cedex, France.

<sup>b</sup> Université Paris-Est, IFSTTAR, Département Matériaux & Structures, 14-52 boulevard Newton, F-77447 Marne la Vallée cedex 2, France.

## Abstract

Describing water transport in concrete is an important issue for the durability assessment of radioactive waste management reinforced concrete structures. Due to the waste thermal output such structures would be submitted to moderate temperatures (up to 80°C). We have then studied the influence of temperature on water transport within hardened cement pastes of four different formulations. Using a simplified approach (describing only the permeation of liquid water) we characterized the properties needed to describe water transport (up to 80°C) using dedicated experiments. For each hardened cement paste the results are presented and discussed.

**Keywords:** Waste management (E) – Cement paste (D) – Drying (A) – Temperature (A) - Permeability (C).

## 17 **1. Introduction**

18 Water plays a very important role in concrete structures durability. This fact is well illustrated by the  
19 results of Tuutti [1] which relate the variations of the corrosion current of steel embedded in a  
20 carbonated mortar as a function of the external relative humidity (RH). In a more general way water is  
21 necessary for the chemical reactions to occur (in solution) and presents a significant impact on concrete  
22 transport properties. The durability assessment of concrete structures thus necessitates an accurate  
23 description of water transport all along service life. Among the data needed to compute water flow in  
24 unsaturated conditions, the water sorption isotherm and permeability are the most important (see part  
25 2). In the field of radioactive waste management, the concrete structures and containers would also  
26 have to cope with heating due to the waste thermal output (the maximal temperature to be reached is  
27 80°C).

28 It has been known for long that water transport is strongly influenced by temperature. Experiments  
29 performed on cementitious materials have shown that the higher the temperature, the faster the water  
30 transport [2-9]. Several authors used the diffusion equation to describe isothermal drying experiments.  
31 In so doing, the resulting moisture diffusivity  $D$  was found to increase with temperature. Glover and  
32 Raask [4] showed the moisture diffusivity of a Portland cement paste (water-to-cement ratio  $w/c = 0.28$ )  
33 was multiplied by 11 to 15 between 30 and 70°C whereas Wong et al. [7] obtained a factor 6 to 8  
34 between 20 and 40°C for three concretes (Portland cement,  $w/c = 0.4, 0.5$  and  $0.6$ ). In the same way  
35 Powers [5] measured the permeability of Portland cement pastes ( $w/c$  from 0.5 to 0.8) between 0 and  
36 27°C using water. The resulting hydraulic conductivity (that depends on water viscosity, in m/s) was  
37 found to increase by a factor 3. Hughes et al. [2] and Hancox [3] dried Portland cement paste samples  
38 ( $w/c = 0.3$  and  $0.5$ ) at temperatures ranging from 21 to 95°C. The diffusivity increase with temperature  
39 was found to follow Arrhenius' equation. The mean activation energy was 43 kJ/mol (10.2 kcal/g/mol).

40 It must be mentioned that smaller increase in water transport properties were obtained in recent  
41 studies. Jooss and Reinhardt [9] measured water permeability and diffusivity of several different  
42 cementitious materials (using water permeametry and cup method). They found that permeability and  
43 diffusivity were only increased by 18-92% and 18-41% respectively between 20 and 80°C. Černý et al. [8]  
44 used the so-called PCK method (similar to an imbibition test) to estimate the moisture diffusivity of two  
45 concrete used for nuclear power plants containment building in France and Czech Republic. The values  
46 obtained at 80°C were greater than the ones obtained at 5°C by a factor 2.0-2.5.

47 Temperature is also known to affect the water retention properties of cementitious materials [6, 10-15].  
48 A temperature increase leads to the reduction of the amount of water retained at equilibrium with a  
49 given RH: the greater the temperature increase, the more the reduction. For instance for a high-  
50 performance concrete kept at 60% RH, increasing temperature from 30 to 80°C led to the reduction of  
51 the water content (by mass) at equilibrium from 3% to about 1% [13]. The isotherm shape is also  
52 modified; the water content reduction is not constant over the RH-range. It depends on the temperature  
53 increase. Another important point is the absence of temperature threshold: any change in temperature  
54 is expected to impact the water retention curve.

55 The influence of temperature is generally attributed to the variation of water physical properties (density  
56 and surface tension) [16] as well as the coarsening of the pore structure in relation to ettringite  
57 dissolution and C-S-H alteration [14]. It was however suggested recently that another phenomenon  
58 might be at work [13]. A temperature change at a constant RH leads to the shift of equilibrium between  
59 the adsorbed phase and water vapor. Since adsorption is an exothermic process, a temperature increase  
60 shifts the equilibrium towards the endothermic reaction (that is to say desorption). Consequently water  
61 is released. A simple tool was then proposed to describe this so-called “thermal desorption” [17]. It is  
62 based on Clausius-Clapeyron equation [18]:

63 
$$q_{st}(w) = -R \left. \frac{\partial \ln(p_v)}{\partial \left(\frac{1}{T}\right)} \right|_w \quad (1)$$

64 where:

- 65 •  $R$  is the universal gas constant (8.3145 J/mol/K);
- 66 •  $p_v$  vapor pressure (Pa) at equilibrium with the water content  $w$ ;
- 67 •  $T$  absolute temperature (K);
- 68 •  $q_{st}$  isosteric energy (J/mol).

69  $q_{st}$  corresponds to the amount of heat involved in the adsorption process (J/mol). Note that in eq. (1) the  
 70 derivation operation must be carried out for a constant amount of adsorbed water  $w$ . The isosteric  
 71 energy  $q_{st}$  can be obtained using two isotherms at two distinct temperatures. Once  $q_{st}$  is known, the  
 72 water retention curve for any arbitrary temperature  $T$  can be easily estimated using:

73 
$$h(w, T) = h(w, T_0) \frac{p_{vs}(T_0)}{p_{vs}(T)} \exp \left[ q_{st}(w) \frac{T - T_0}{RTT_0} \right] \quad (2)$$

74 where:

- 75 •  $p_{vs}(T)$  is the vapor pressure at saturation (Pa) for the absolute temperature  $T$ ;
- 76 •  $h(w, T)$  relative humidity at equilibrium with the water content  $w$  at the absolute temperature  $T$ .

77 This simple model was found to satisfactorily reproduce the temperature-induced evolution of concrete  
 78 water retention curve [13, 17]. This model implicitly assumes that the shift of equilibrium is the only  
 79 mechanism at work and that the microstructure modifications can be neglected.

80 For the description of unsaturated water transport, the intrinsic permeability is commonly evaluated  
 81 through inverse analysis [19-22]: the temperature-induced modifications of the water retention curve  
 82 described above are then expected to have a significant influence on the permeability assessment [23].

83 The main objective of this study was to assess the influence of temperature on unsaturated permeability.

84 With regards to Andra's (the French agency for radioactive waste management) requirements in the  
85 context of nuclear waste storage, we have designed an experimental campaign to acquire all the data  
86 needed to describe unsaturated water transport using a simplified model (see section 2) and  
87 cementitious materials of interest. The results do constitute a unique and consistent dataset.

## 88 **2. Background**

89 Water transport within porous media involves three different motions: (1) permeation of the liquid  
90 water; (2) permeation of the gaseous phase (water vapor + dry air) and (3) diffusion of water vapor  
91 within the gaseous phase. The neat description of these phenomena leads to three coupled differential  
92 equations [20, 21, 24-27]. The major drawback of such an approach is the very large number of input  
93 data that are difficult to acquire experimentally.

94 From a practical point of view, water transport can be profitably described in a simplified way using a  
95 single equation accounting for liquid permeation only. The others motions (permeation of the gaseous  
96 phase and water vapor diffusion) are neglected. This assumption was found to be valid for a hardened  
97 cement paste ( $w/c = 0.35$ ) with a permeability equal to  $1.0 \times 10^{-21} \text{ m}^2$  [20]. In a recent study Thiery et al.  
98 [28, 29] estimated the respective contribution of each motion to the overall water flow. They showed  
99 that the assumption validity domain depends on the material properties and especially on permeability.  
100 For a high-performance concrete ( $w/c = 0.27$ ) with low permeability ( $2 \times 10^{-22} \text{ m}^2$ ) the assumption is valid  
101 between  $RH=20\%$  and  $100\%$  whereas it is only valid between  $RH=65\%$  and  $100\%$  for a low-strength  
102 concrete ( $w/c = 0.84$ ) with high permeability ( $4 \times 10^{-19} \text{ m}^2$ ).

103 The liquid water flow rate is given by the extension of Darcy's law for incompressible unsaturated media  
104 [30]:

105 
$$\underline{j}_w = -\rho \frac{K}{\eta} k_r \text{grad}(P), \quad (3)$$

106 In which:

- 107 •  $\eta$  is the water viscosity [Pa s];  
108 •  $\rho$  water density [kg/m<sup>3</sup>];  
109 •  $K$  intrinsic permeability [m<sup>2</sup>];  
110 •  $k_r$  relative permeability to water [without unit];  
111 •  $P$  water pressure [Pa].

112 In unsaturated conditions the water pressure presents negative values  $P \in ]-\infty ; 0]$ . It is evaluated using  
113 Kelvin-Laplace equation:

114 
$$P = -\rho \frac{RT}{M} \ln(h), \quad (4)$$

115 where  $M$  is the water molar mass [0.018 kg/mol].

116 The mass conservation equation writes:

117 
$$\frac{\partial}{\partial t} (\rho \emptyset S) = -\text{div}(\underline{j}_w) = -\text{div}\left[-\rho K \frac{k_r}{\eta} \text{grad}(P)\right], \quad (5)$$

118 In which

- 119 •  $S$  is the saturation index [without unit], it characterizes how pores are filled (by volume) with  
120 liquid water. It ranges between 0 (dry state) and 1 (saturated state).  
121 •  $\emptyset$  is the concrete porosity [volume per volume, without unit].

122 In isothermal conditions (as this is the case in this study, see after) and assuming that water is  
123 incompressible and that water flow is the only phenomenon at work (absence of dissolution or  
124 precipitation),  $\rho$  and  $\emptyset$  can be considered as constants. The following equation is obtained:

125 
$$\phi \frac{\partial S}{\partial t} = \text{div} \left[ K \frac{k}{\eta} \text{grad}(P) \right] \quad (6)$$

126 Assuming that a differentiable function exists between water saturation  $S$  and pressure  $P$  one can obtain:

127 
$$\phi \left( \frac{\partial S}{\partial P} \right) \frac{\partial P}{\partial t} = \text{div} \left[ K \frac{k}{\eta} \text{grad}(P) \right] \quad (7)$$

128 This simple equation allows the water transport description within the cementitious materials knowing  
 129 only four their properties, namely: the porosity  $\phi$ , the derivative of the capillary pressure function, the  
 130 intrinsic and relative permeability  $K$  and  $k_r$ . Following Savage and Janssen [31] the water retention curve  
 131 is almost described using the equation proposed by van Genuchten [32]:

132 
$$S = \left[ 1 + \left( \frac{|P|}{P_0} \right)^{\frac{1}{1-m}} \right]^{-m} \quad (8)$$

133 where  $P_0$  and  $m$  are two positive parameters:  $m$  (usually around 0.5) [without unit] whereas  $P_0$  is  
 134 equivalent to a pressure [several tenths of MPa]. The use of Mualem's model [33] together with eq. (8)  
 135 allows deriving an analytical expression for the relative permeability  $k_r$  (the value of the parameters  $m$   
 136 and  $P_0$  are the same as above):

137 
$$k_r = \sqrt{S} \left[ 1 - \left( 1 - S^{\frac{1}{m}} \right)^m \right]^2 = \left[ 1 + \left( \frac{|P|}{P_0} \right)^{\frac{1}{1-m}} \right]^{-\frac{m}{2}} \left\{ 1 - \left( \frac{|P|}{P_0} \right)^{\frac{1}{1-m}} \left[ 1 + \left( \frac{|P|}{P_0} \right)^{\frac{1}{1-m}} \right]^{-m} \right\}^2 \quad (9)$$

138 The left-hand term  $\left( \frac{\partial S}{\partial P} \right)$  of equation (7) is given by:

139 
$$\left( \frac{\partial S}{\partial P} \right) = \frac{m}{(m-1)P_0} \left( \frac{|P|}{P_0} \right)^{\frac{1}{1-m}} \left[ 1 + \left( \frac{|P|}{P_0} \right)^{\frac{1}{1-m}} \right]^{-1-m} \quad (10)$$



## 140 **3. Methods**

### 141 **3.1. Materials**

142 We used hardened cement pastes prepared using four different binders that were selected for their  
143 potential interest for radioactive waste management in France:

- 144 • The CEM I 52.5 R CE PM-ES-CP2 (according to the European standard EN-206) from Val  
145 d’Azergues factory (France, Lafarge). This ordinary Portland cement (OPC) was selected by Andra  
146 (the French Agency for radioactive waste management) as a reference cement for the study of  
147 concrete structures and waste packages.
- 148 • The CEM II/B-LL 42.5 N CE CP2 from Le Teil factory (France, Lafarge). This cement (OPC + 25%  
149 limestone filler) was selected because it was used for the realization of a scale-one subsurface  
150 storage structure mockup (Galatée) [34-36].
- 151 • The CEM V/A (S-V) 42.5 N CE PM-ES-CP1 from Airvault factory (Calcia, France). This cement was  
152 selected by Andra as a reference binder for concrete packages.
- 153 • A low-alkalinity ternary mix of CEM I/OPC (37.5%), silica fume (32.5%) and fly ash (35%). The  
154 cement used in this mix was provided by Lafarge, Le Teil factory, France (CEM I 52.5 N CE PM-  
155 ES). The silica fume and fly ash were provided by Condensil (S 95 DM) and Calcia respectively.  
156 This mix composition was designed in the field of geological disposal by [37, 38] to mitigate the  
157 heat emitted during hydration and limit the chemical interaction between clay minerals and  
158 concrete parts (alkaline plume) which could impair clay physical and chemical properties.

159 A unique water-to-binder ratio (w/b) was used to enable comparison between the four pastes. We chose  
160 w/b = 0.40 because it allowed the CEM I paste to be representative of the concrete studied in [13]. The  
161 resulting hardened cement paste is the same as the one embedding the concrete aggregates. For this

162 purpose, the paste water to binder ratio w/b was adjusted to account for the water brought by the  
 163 superplasticizer and absorbed by the aggregates. Moreover this value appeared to yield good properties  
 164 of each fresh paste (good workability, neither visible segregation nor bleeding). The composition of each  
 165 paste is given in Table 1.

166 *Table 1. Composition of the pastes.*

Compound	CEM I	CEM II	CEM V	Low-pH	Unit
OPC	1396	1023	759	468	g/L of paste
Calcareous filler	-	341	-	-	g/L of paste
Slag	-	-	298	-	g/L of paste
Fly ash	-	-	298	377	g/L of paste
Silica fume	-	-	-	405	g/L of paste
Water	558	545	542	500	g/L of paste
Superplasticizer	-	-	-	12.5	g/L of paste

167

168 The four pastes were prepared in the laboratory in ten consecutive batches (two liters each) spanning  
 169 over three days. Each specimen was cast in a cylindrical mold ( $\varnothing 35 \times H60$  mm for water adsorption  
 170 experiments and  $\varnothing 51 \times H80$  mm for permeability assessment experiments) which was then hermetically  
 171 closed and kept at 20°C for seven days before unmolding. All the specimens of the same formulation  
 172 were immersed in a special curing solution inside an air-tight chamber (to prevent carbonation) for three  
 173 months. The composition of the curing solution was adjusted to prevent calcium and alkalis leaching. For  
 174 the CEM I, CEM II and CEM V pastes we determined the curing solution composition by expression of the  
 175 pore solution [39] and analysis using ionic chromatography (Table 2). The samples used for extraction  
 176 were kept three months in sealed bags (rather than under water to prevent dilution of the alkalis).  
 177 Analysis of the solutions at the beginning and end of the cure showed limited change (Table 2).

178 *Table 2. Composition of the interstitial solutions (in mmol/L) and pH of the curing solutions before and*  
 179 *after cure of the CEM I CEM II and CEM V pastes.*

	CEM I				CEM II/B				CEM V/A			
	Na <sup>+</sup>	K <sup>+</sup>	Ca <sup>2+</sup>	pH	Na <sup>+</sup>	K <sup>+</sup>	Ca <sup>2+</sup>	pH	Na <sup>+</sup>	K <sup>+</sup>	Ca <sup>2+</sup>	pH
Interstitial solution	47	452	2	13.7	91	94	1	13.2	87	533	2	13.7
Beginning of cure	49	439	2	13.6	90	93	3	13.3	90	518	4	13.7
End of cure	54	455	3	13.6	96	95	5	13.2	85	474	2	13.7

180

181 The sodium content of the three cements is quite low (and especially in comparison to the potassium  
 182 content). This is a direct consequence of the cements composition, low in sodium (Table 3).

183 *Table 3. Chemical composition of the cements.*

	SiO <sub>2</sub>	Al <sub>2</sub> O <sub>3</sub>	Fe <sub>2</sub> O <sub>3</sub>	CaO	MgO	SO <sub>3</sub>	K <sub>2</sub> O	Na <sub>2</sub> O	MnO	TiO <sub>2</sub>	LOI	INS
CEM I	21.0	3.4	4.5	65.0	0.62	2.7	0.72	0.09	-	-	1.3	0.2
CEM II/B	18.0	3.5	1.7	62.6	0.85	2.97	0.16	0.15	-	-	9.4	1.2
CEM V/A	30.0	11.2	3.6	46.4	2.75	2.8	1.16	0.2	0.1	0.6	2.1	-

184

185 For the Low-pH which pore solution is known to exhibit great concentration variations in the first months  
 186 of hydration (portlandite is gradually consumed to precipitate new C-S-H: portlandite completely  
 187 disappears after two months) [38], a different approach was chosen. Several samples were reduced into  
 188 a rough powder and added to deionized water to generate the curing solution.

189 After the curing period, both ends (top and bottom) of each sample were sawn (using a diamond wire  
 190 saw with water) and discarded. This resulted in smaller cylinders (Ø35×H50 mm for water adsorption  
 191 experiments and Ø51×H60 mm for permeability assessment experiments) that were assumed to present  
 192 homogeneous properties versus height [40-42]. Because the specimens were kept under water for three  
 193 months after casting, full saturation at the cure end was assumed: no additional procedure was thus

194 used to ensure initial saturation (for instance saturation under vacuum). It was however verified on a few  
195 samples that no water uptake was observed after 48 hours under water and vacuum.

### 196 **3.2. Mineralogical composition**

197 The portlandite content was measured using thermogravimetric analysis (TGA). Just after the cure, a  
198 specimen was powdered in a CO<sub>2</sub>-free glove box and 120 mg ( $\pm$  1 mg) were placed in an automated TG  
199 analyzer (Netzsch STA 409 PC). The temperature was increased at constant rate (10 °C/min) under dry  
200 nitrogen flowrate (60 mL/min). The portlandite content was computed using the mass loss obtained  
201 between 400 and 600°C.

202 The C-S-H concentration was estimated following the approach of Olson and Jennings [43] that relates  
203 the amount of water adsorbed at 20% RH to the C-S-H content. It was then implicitly assumed that the  
204 calcium-to-silicon (C/S) ratio of the C-S-H was equal to 1.7. We took advantage of the experimental water  
205 retention curves to assess the water content at equilibrium at 20%. The model proposed by Pickett [44]  
206 was fitted to the experimental results and used to compute the water content at 20% (see part 3.4.).

### 207 **3.3. Porosity and microstructure**

208 The specific gravity of the saturated materials  $d_s$  was measured using the buoyancy method following  
209 current recommendations (French standard P18-459:2010): the saturated specimens were weighed  
210 under water and in air (using a 1 mg accurate device). In air, the water in excess on the specimen surface  
211 was removed using a wet cloth. The measurements were done in an air-conditioned room ( $20 \pm 2^\circ\text{C}$ ).

212 The porosity to water  $\phi$  (by volume) was determined by oven-drying until constant weight; different  
213 drying temperatures were used from 20°C to 105°C for comparison purposes. At 20°C and 50°C we used  
214 silica gel as desiccant (RH  $\approx$  3%) whereas calcium chloride proved to be much more efficient at 80°C (RH  
215 measured at 0.0% using capacitive hygrometer). No desiccant was used at 105°C (the RH decrease

216 induced by heating at 105°C is high enough). A different five-sample set was used for each configuration.  
 217 Due to the great number of sample-sets all the five specimens were weighed together; this explains why  
 218 there is no variability information in this case (no standard deviation).

219 The pore-size distribution was characterized using mercury intrusion porosimetry (MIP). Some specimens  
 220 were first kept a few months in sealed containers above silica gel (at 20°C and 50°C) or calcium chloride  
 221 (at 80°C) to remove most of the evaporable water. They were crushed into pieces (several millimeters  
 222 thick), freeze-dried using liquid nitrogen and eventually tested (up to 414 MPa). Three or four replicates  
 223 were tested for each experiment.

224 The specific surface area of each paste was assessed either directly by MIP or by post-processing the  
 225 experimental water desorption isotherms using the linear form of the BET model [45]:

$$226 \quad \frac{h}{(1-h)w} = \frac{1}{C^B w_m^B} + \frac{C^B - 1}{C^B w_m^B} h \quad (11)$$

227 where  $C^B$  and  $w_m^B$  are the two BET parameters.  $C^B$  is related to the energy of the first adsorbed layer and  
 228  $w_m^B$  is the water content needed to complete a monomolecular layer. The BET linear form was used to  
 229 check the validity domain (for which the experimental points follow a straight line). The specific surface  
 230 area  $S_S$  was evaluated using the BET monolayer values  $w_m^B$  using [46]:

$$231 \quad S_S = N_A \frac{A_w}{\rho V} w_m^B \quad (12)$$

232 where  $N_A$  is Avogadro's number ( $N_A = 6.02 \times 10^{23} \text{ mol}^{-1}$ );  $V$  is water molar volume ( $V = 1.80 \times 10^{-5} \text{ m}^3/\text{mol}$  at  
 233 20°C) and  $A_w$  is the surface area occupied by one water molecule on the sample surface. It was estimated  
 234 using [47, 48]:

$$235 \quad A_w = 1.091 \left( \frac{M}{\rho N_A} \right)^{\frac{2}{3}} \quad (13)$$

236 **3.4. Water retention curves**

237 They were characterized in a classical way using the desiccator method [49] following the protocol used  
238 in [13]. Four cylinders ( $\varnothing 35 \times H 50$  mm) of each formulation were put in a desiccator above a saturated salt  
239 solution for RH control (sixteen specimens were then introduced into the same desiccator). The  
240 specimen dimensions may seem big, but the low specific surface area of the specimens allowed us not to  
241 take any precaution against carbonation and to limit the potential impact of sawing (superficial cracking).  
242 The main disadvantage was the increase of the time needed to reach hygral equilibrium. We then  
243 determined the whole desorption isotherm for each paste by submitting different sets of specimens to  
244 different RHs (using different desiccators) simultaneously rather than submitting a unique set to  
245 decreasing RH steps. This was expected to induce some variability but it allowed reducing drastically the  
246 whole experiment duration.

247 This experiment was conducted at 20, 50 and 80°C. At 20°C, the desiccators were kept in an air-  
248 conditioned room ( $20^\circ\text{C} \pm 2^\circ\text{C}$ ) whereas ovens were used for the two other temperatures: three different  
249 ovens were used for 50°C and two for 80°C. At 50°C the regulation did not appear to be fully satisfactory:  
250 the temperature in the three ovens was found to be ranging from 50 to 60°C. This is believed to have  
251 induced some variability in the isotherm characterization. At 80°C, the temperature variability was far  
252 less than 1°C. The salt solutions used and the resulting RHs are reported in Table 4.

253 *Table 4. Relative humidity as a function of temperature and saturated salt solution [50-54].*

Saturated salt solutions		Temperature		
		20°C	50°C	80°C
Calcium chloride	CaCl <sub>2</sub>	5%	3%	≈0%
Silica gel	SiO <sub>2</sub>	3%	3%	≈10%
Lithium chloride	LiCl	11%	11%	11%
Magnesium chloride	MgCl <sub>2</sub>	33%	31%	26%
Potassium carbonate	K <sub>2</sub> CO <sub>3</sub>	43%	-	-
Magnesium nitrate	Mg(NO <sub>3</sub> ) <sub>2</sub>	54%	-	-

Sodium bromide	NaBr	59%	51%	51%
Urea	CO(NH <sub>2</sub> ) <sub>2</sub>	-	62%	-
Ammonium nitrate	NH <sub>4</sub> NO <sub>3</sub>	63%	-	-
Potassium iodide	KI	70%	64%	61%
Sodium nitrate	NaNO <sub>3</sub>	-	69%	65%
Sodium chloride	NaCl	-	74%	76%
Ammonium sulfate	(NH <sub>4</sub> ) <sub>2</sub> SO <sub>4</sub>	-	79%	-
Ammonium chloride	NH <sub>4</sub> Cl	80%	-	-
Potassium chloride	KCl	-	-	80%
Potassium nitrate	KNO <sub>3</sub>	-	85%	-
Sodium carbonate	Na <sub>2</sub> CO <sub>3</sub>	-	-	85%
Barium chloride	BaCl <sub>2</sub>	90%	-	-
Sodium sulfate	Na <sub>2</sub> SO <sub>4</sub>	-	-	90%
Potassium sulfate	K <sub>2</sub> SO <sub>4</sub>	98%	96%	95%
Deionized water	H <sub>2</sub> O	100%	100%	100%

254

255 Periodically we opened each desiccator, weighed each specimen-set (weighing each sample would have  
 256 been too much time-consuming) and computed the corresponding relative mass variation to monitor  
 257 sample drying:

$$258 \quad \left(\frac{\Delta m}{m}\right)(t) = \frac{m(t) - m(t_0)}{m(t_0)} \quad (14)$$

259 where  $m(t)$  is the mass for the time  $t$  and the mass for the time  $t_0$  corresponds to the experiment  
 260 beginning). The difference from equilibrium was characterized using the following indicator  $\varepsilon$  which is an  
 261 estimator of the relative mass variation curve slope:

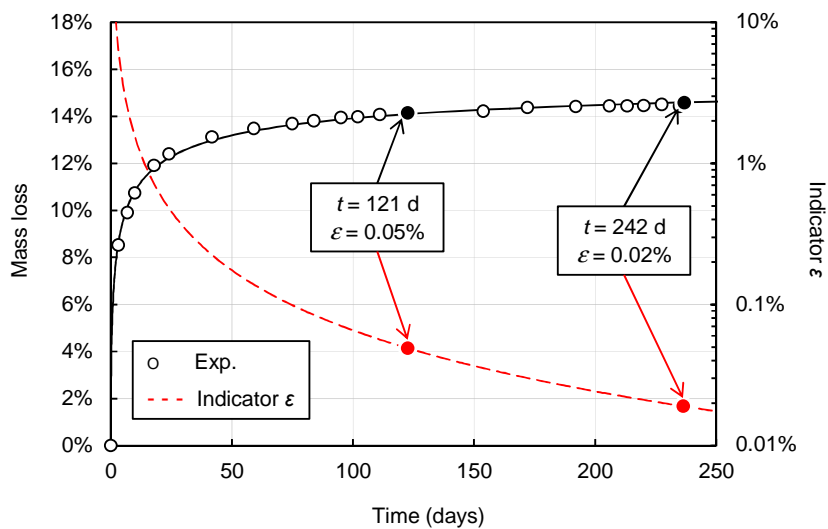
$$262 \quad \varepsilon(t) = \frac{\left(\frac{\Delta m}{m}\right)(t+1) - \left(\frac{\Delta m}{m}\right)(t)}{\left(\frac{\Delta m}{m}\right)(t)} \quad (15)$$

263 where  $\left(\frac{\Delta m}{m}\right)(t)$  and  $\left(\frac{\Delta m}{m}\right)(t + 1)$  are the relative mass variations at time  $t$  and one day after respectively.

264 From a practical point of view the  $\varepsilon$  values were estimated using the equation proposed by Baroghel-  
 265 Bouny [55] to fit the sample mass loss evolution:

$$266 \quad \left(\frac{\Delta m}{m}\right)(t) = \frac{A\sqrt{t}}{B + \sqrt{t}} \quad (16)$$

267 where  $A$  and  $B$  are two parameters to be fitted on the experimental results. The samples were let to  
 268 equilibrate in their containers as long as possible but they all met the following requirement:  $\varepsilon \leq 0.05\%$   
 269 (note that many sets of specimens presented lower  $\varepsilon$  values at the end of the test). A graphical  
 270 illustration of this requirement significance is presented on Figure 1 for the CEM I specimens kept at  $80^\circ\text{C}$   
 271 and  $76\%$  RH. The criterion was reached after 121 days. Leaving the samples for 121 more days (the  
 272 equilibration time was then increased by 100%) brought little improvement: the difference between the  
 273 relative mass variations at 121 and 242 days is about 3.5% (relative value). This value was found to be  
 274 lower than the variability induced by the use of a different sample-set for each RH. The resulting  $\varepsilon$  value  
 275 was then 0.02%.



276  
 277 *Figure 1. Illustration of the criterion  $\varepsilon \leq 0.05\%$  for the CEM I paste kept at  $80^\circ\text{C}$  and  $76\%$  RH (in this*  
 278 *example  $A=-16.04\%$  and  $B=1.522 d^{0.5}$ ). Note the log-scale for the indicator  $\varepsilon$ .*

279  
 280 Once the equilibrium was reached for all the sets of specimens (that is to say when  $\varepsilon$  was lower than  
 281  $0.05\%$ ), the desorption isotherm could be evaluated using the initial properties (specific gravity  $d_s$  and



282 porosity  $\emptyset$ ) and the relative mass variations at equilibrium. It was found convenient to describe the  
283 pastes saturation state using the water content  $w$  which is defined as the ratio of water to dry solid by  
284 mass. In our case it could be easily calculated using the following equation:

$$285 \quad w(T, h) = \frac{d_s}{d_s - \emptyset} \left[ \frac{\emptyset}{d_s} + \left( \frac{\Delta m}{m} \right) (T, h) \right] \quad (17)$$

286 where  $\left( \frac{\Delta m}{m} \right) (T, h)$  is the relative mass variation at equilibrium with the relative  $h$  for the temperature  $T$ .

287 To ensure comparison between the desorption isotherm for the three temperatures a common  
288 reference dry state is necessary because temperature affects the free water amount. For instance drying  
289 at 20°C using silica gel (RH=3%) as proposed by Baroghel-Bouny [19, 56] is unsuitable here. It is known  
290 that heating at 80°C is harmful for cementitious materials mineralogy and microstructure [57-60]. Yet as  
291 far as only the first desorption is concerned (no preliminary drying and no further resaturation) drying at  
292 80°C (using CaCl<sub>2</sub>) was chosen here for commodity. In so doing, it was implicitly assumed that the  
293 80°C-induced degradation influence on total porosity could be neglected. The authors acknowledge that  
294 drying at 80°C is not the common procedure. The reader should remind that porosity was also measured  
295 using different protocols (Table 8) and it is possible to use eq. (18) to recalculate the desorption  
296 isotherms (for instance 105°C).

297 Two different models were used to fit the desorption isotherms: Mualem-van Genuchten equation (eq.  
298 8) was used for unsaturated water transport and Pickett's model was used for adsorption physics. The  
299 model proposed by Pickett is considered by the authors to be the only simple model describing the  
300 physics of adsorption that can efficiently fit the results (type IV isotherms). Using a model based on  
301 adsorption physics instead of that of van Genuchten also proved to ensure a better estimation of the  
302 water content at 20% and isosteric energy  $q_{st}$ . Pickett's equation is an evolution of the well-known BET  
303 model. It can be written under the following form:

304 
$$w = C^P w_m^P \frac{(1-h^n)h + bn h^n(1-h)}{(1-h)[(1-h) + C^P(h + b h^n)]}$$
 (18)

305 where:

- 306 •  $C^P$  is a positive constant that is related to the energy of adsorption of the first layer;
- 307 •  $w_m^P$  the monolayer value corresponds to the water content that is needed to complete a
- 308 monomolecular layer;
- 309 •  $n$  represents the maximal number of adsorbed layers;
- 310 •  $b$  is related to the rate of evaporation/condensation of water molecules in the layers.

311 **3.5. Permeability assessment**

312 We did not measure directly the intrinsic permeability  $K$  (m<sup>2</sup>), for instance using water permeametry [61]  
 313 because such results are known to be unsuitable for the simulation of unsaturated water flow in  
 314 concretes [22]. The intrinsic permeability was rather evaluated through inverse analysis as already  
 315 proposed [20, 21]. For this purpose, the biggest cylinders (Ø51×H60 mm) were put in climatic chambers  
 316 using the constant environmental conditions reported in Table 5. Periodically the chambers were opened  
 317 and the samples weighed. The tests were conducted for 65 days for 20°C and 14 days for 50 and 80°C  
 318 respectively.

319

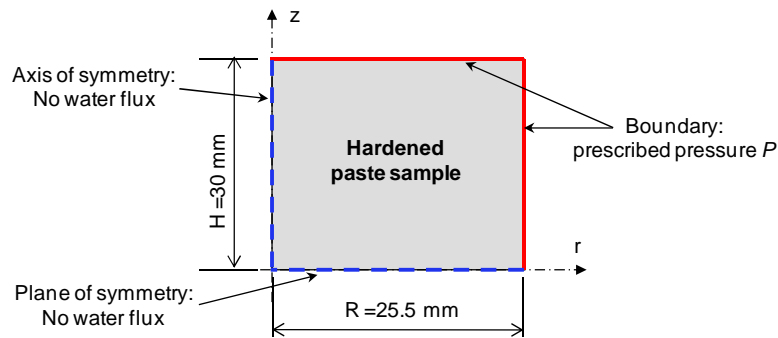
320 *Table 5. Tests conditions for intrinsic permeability assessment tests.*

Temperature	20°C	50°C	80°C	Unit
RH	54%	85%	85%	-
Liquid pressure (eq. 4)	-83.29	-23.96	-25.78	MPa
Duration	65	14	14	days

321

322 The experimental mass variations were then described using the simplified approach detailed in part 2.  
323 From a practical point of view, the finite-element code Cast3m<sup>1</sup> was used to solve eq. (7) and compute  
324 the resulting theoretical mass variation. Different intrinsic permeability values were used and the best  
325 value was selected using a least-squares minimization process. For more detail about the fitting process  
326 the reader is referred to [23]. A quarter of the specimen was described in axisymmetric conditions  
327 (Figure 2). 7200 four-node quadrangles (80×90) were used. The time steps were adjusted to ensure  
328 convergence (from a few seconds at the beginning of the simulations to one day at the end).

329



331 *Figure 2. Schematic description of the numerical simulations for permeability assessment.*

332

333 The heating stage was not described (the temperature was assumed to be constant). The initial  
334 conditions were: uniform temperature (20, 50 or 80°C) and liquid pressure  $P=0.0$  MPa (saturation). At  
335  $t=0$ , a constant pressure (Dirichlet condition) was prescribed all over the sample boundary (the  
336 corresponding values are listed in Table 5).

---

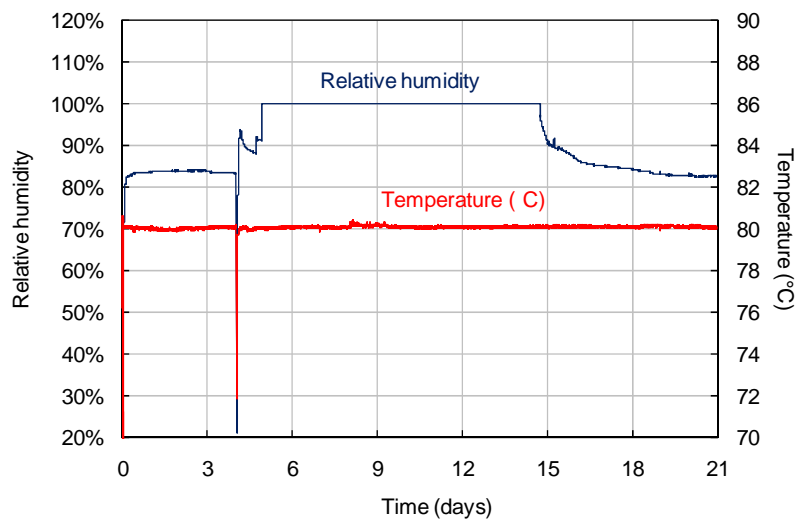
<sup>1</sup> <http://www.cast3m.org>

337 **4. Results**

338 **4.1. Feedback on the use of saturated salt solutions**

339 Two major drawbacks were encountered when using saturated salt solutions. First, we did not find this  
340 method to be successful for RH regulation: a good illustration is given on Figure 3. We prepared a sodium  
341 carbonate ( $\text{Na}_2\text{CO}_3$ ) solution in a four-liter desiccator (the same kind as the ones used for the water  
342 retention curve characterization) and left it four days in an oven at  $80 \pm 1^\circ\text{C}$ . Temperature and RH were  
343 constantly recorded using a commercial hygrometer: the RH target (85%, Table 4) was quickly reached.  
344 After four days, we opened the desiccator and introduced four (saturated) paste specimens. The RH  
345 within the desiccator then quickly increased to reach saturation (100%) due to the water release by the  
346 four specimens. The RH only began to decrease 11 days after the samples introduction and returned to  
347 the target value 14 days after.

348



349

350 *Figure 3. RH and temperature evolution within a desiccator after the insertion of four paste samples (the*  
351 *salt used is  $\text{Na}_2\text{CO}_3$  resulting in RH=85% at  $80^\circ\text{C}$ ).*

352

353 In this example, only four specimens were introduced whereas sixteen of them were used in the water  
354 retention curve experiments. In so doing, we did not expect the salt solutions to successfully maintain  
355 the RH in the short term for the three tested temperatures. We believe that it did result in increasing the  
356 time needed to reach equilibrium: the resulting mass loss evolutions of the specimens could not be used  
357 for water transport properties evaluation. This explains why supplementary isothermal drying tests were  
358 conducted for permeability assessment. In a more general way, when using saturated salt solutions to  
359 maintain constant conditions one should at least monitor the RH evolution or if possible adjust the  
360 chamber volume to the specimens water release rate and salt used.

361 The second major problem we had to face was the crystallization of salt above the solution on the  
362 desiccator walls which could eventually come in contact with the specimens and result in unacceptable  
363 pollution. This was believed (but it was not verified) to be due to the handling operations needed to have  
364 the samples weighed (periodical withdrawal from the oven which could project some solution on the  
365 desiccator walls) and to the supersaturation induced by the solution cooling and drying (due to the  
366 desiccator opening). This was hindered by periodical examination (twice a week) of all the desiccators to  
367 check the salt crystallization. When present, the desiccator walls were thoroughly rinsed and dried using  
368 pure water and a clean towel. When the time between two remediation operations was too small, both  
369 desiccator and salt solution were eventually changed. The salts under discussion are sodium bromide  
370 (NaBr) which was found to be difficult to use at 50 and 80°C whereas sodium chloride (NaCl), potassium  
371 chloride (KCl) and to a lesser extent magnesium chloride (MgCl<sub>2</sub>) were only troublemaking at 80°C.

#### 372 ***4.2. Mineralogical composition***

373 The contents of portlandite and C-S-H of each paste are presented on Table 6. The CEM I and CEM II  
374 pastes showed pretty similar results (despite the limestone filler substitution). As expected, the Low-pH

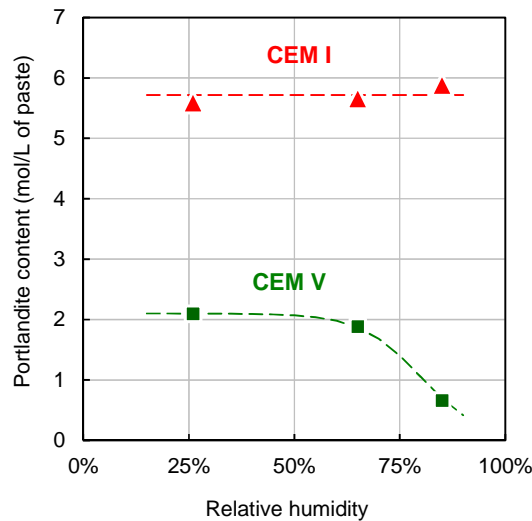
375 mix was free of portlandite as already observed by Codina et al. [38]. As a consequence of pozzolanic  
 376 reactions, the C-S-H content was high (7.4 mol/L). The CEM V paste laid between the CEM I and the Low-  
 377 pH pastes (2.1 mol/L).

378 *Table 6. Portlandite and C-S-H contents of the pastes after the cure.*

Phase	CEM I	CEM II	CEM V	Low-pH	Unit
Portlandite	5.6	5.4	2.1	0.0	mol/L of paste
C-S-H	5.1	5.0	7.0	7.4	mol/L of paste

379

380 A few TGA tests were also conducted using some of the specimens kept at 80°C (and CaCl<sub>2</sub>) for the  
 381 desorption isotherm characterization. The portlandite content of the CEM I paste was found to be almost  
 382 constant versus RH whereas that of the CEM V paste decreased when RH was increased. This was taken  
 383 as an indication of ongoing hydration (due to pozzolanic reactions) in the case of the blended cements  
 384 (CEM V and Low-pH). We believe that this might have had an impact on the resulting water retention  
 385 curves (especially at high RH and temperature) but we were unable to quantify it.



386

387 *Figure 4. Portlandite content of the CEM I and CEM V pastes kept at 80°C (dashed lines are guides for the*  
 388 *eye only).*

389 **4.3. Porosity and microstructure**

390 The specific gravity of the saturated pastes  $d_s$  was measured using 134 specimens for each paste (Table  
 391 7). The mean values span from 1.73 (Low-pH) to 2.04 (CEM I): the value decreases when the amount of  
 392 supplementary cementing materials is increased. Table 8 summarizes the porosity results: the higher the  
 393 temperature, the higher the porosity. Yet whatever the drying temperature, the porosity value increases  
 394 with the amount of SCM. Table 9 presents the specific surface area values obtained for each paste using  
 395 MIP and the desorption isotherms (BET). Here again, the value of the specific surface area increases with  
 396 the amount of SCM in relation to the increased C-S-H content. The value obtained using the BET model is  
 397 always significantly higher than that of MIP.

398 *Table 7. Specific gravity of the pastes (standard deviation in brackets).*

Paste	CEM I	CEM II	CEM V	Low-pH
Saturated specific gravity $d_{sat}$	2.04 (0.01)	1.99 (0.01)	1.93 (0.01)	1.73 (0.01)

399

400 *Table 8. Porosity as a function of drying temperature.*

Temperature	Desiccant	RH	CEM I	CEM II	CEM V	Low-pH
20°C	SiO <sub>2</sub>	≈3%	30.4%	31.0%	28.5%	32.1%
50°C	SiO <sub>2</sub>	≈3%	35.2%	35.9%	34.2%	40.3%
80°C	CaCl <sub>2</sub>	≈0%	37.2%	39.5%	38.9%	41.3%
105°C	-	-	38.5%	40.4%	39.1%	45.7%

401

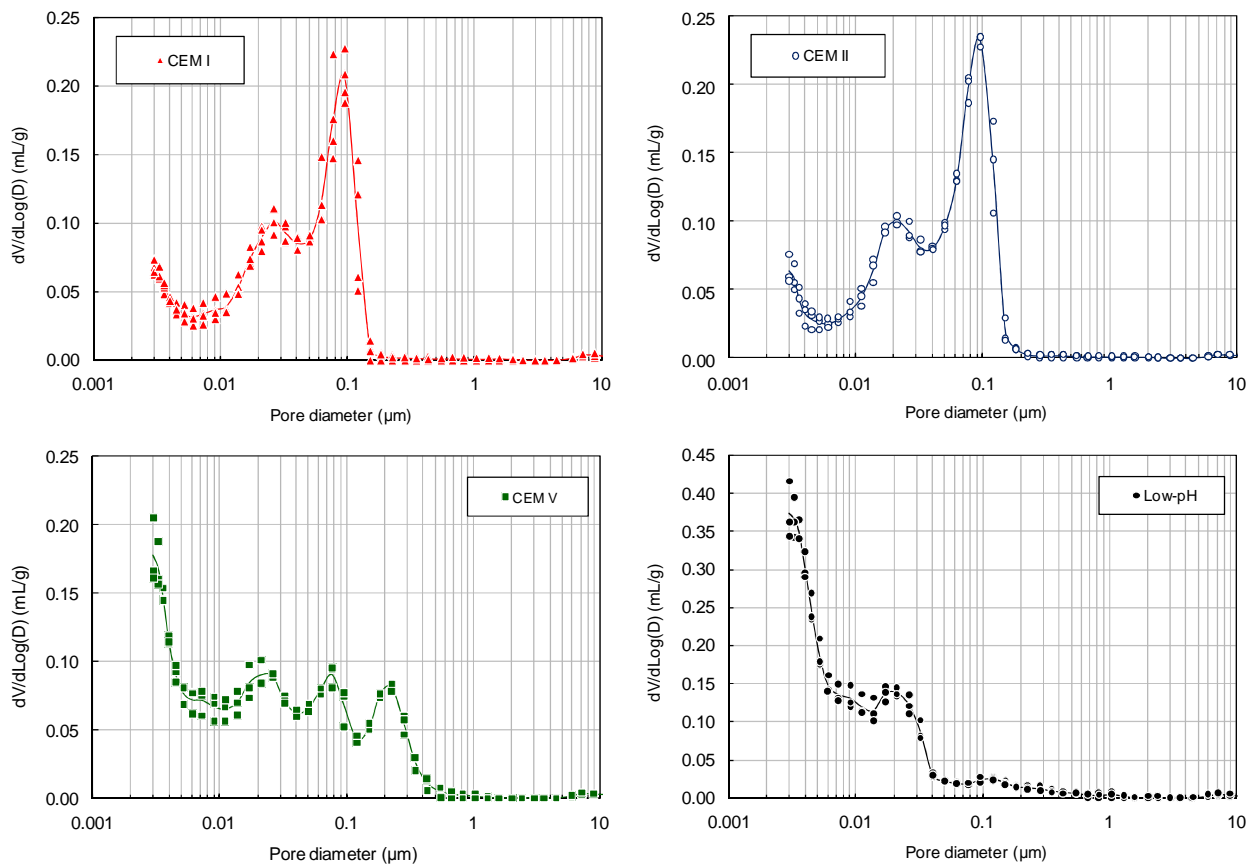
402 *Table 9. Specific surface area of the four pastes.*

Paste	CEM I	CEM II	CEM V	Low-pH	Unit
Specific surface area (BET)	190	199	297	380	m <sup>2</sup> /g
Specific surface area (MIP)	30	31	59	113	m <sup>2</sup> /g

403

404 The MIP results are presented on Figure 5. The CEM I & CEM II pastes exhibited almost the same pore-  
 405 size distribution. The CEM V and Low-pH pore-size distributions showed an important reduction of the  
 406 pores of diameter larger than 50 nm (despite the presence of an unexpected and unexplained pore  
 407 population around 200 nm for the CEM V) together with an important increase of pores of diameter  
 408 lower than 50 nm. This was attributed to the presence of SCMs in the CEM V and Low-pH mix leading to  
 409 supplementary C-S-H formation (see Table 6).

410



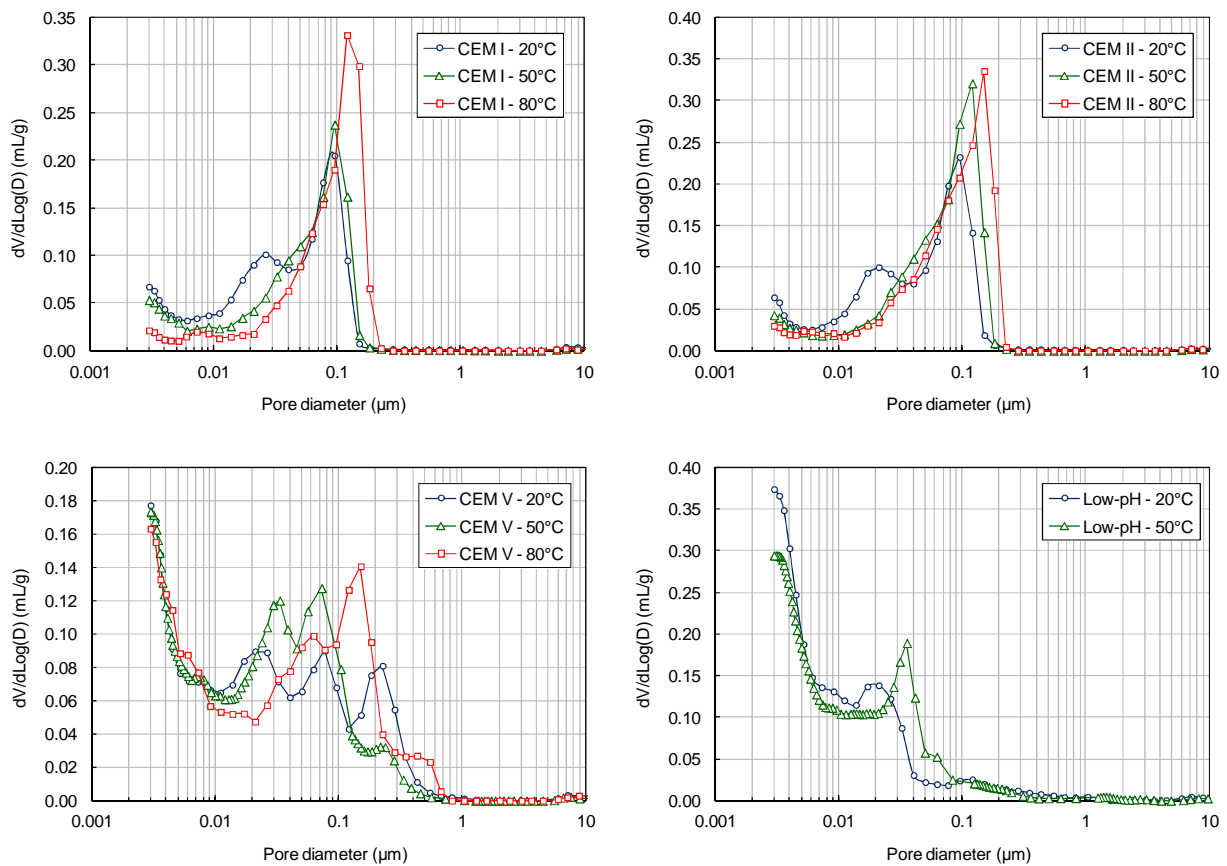
411 *Figure 5. Pore-size distribution of the four hardened cement pastes as obtained using MIP and samples*  
 412 *dried at 20°C (using silica gel and then freeze-drying).*

413



414 The MIP results obtained using heated specimens are depicted on Figure 6. Whatever the considered  
 415 paste, heating led to the coarsening of the pore structure: that is to say the increase of both capillary  
 416 porosity and critical pore radius (corresponding to the sudden slope change in the MIP results). As  
 417 suggested by Brue et al. [14] ettringite dissolution [62, 63] as well as C-S-H alteration [64-66] can be  
 418 considered as the major causes of the pore structure modifications.

419

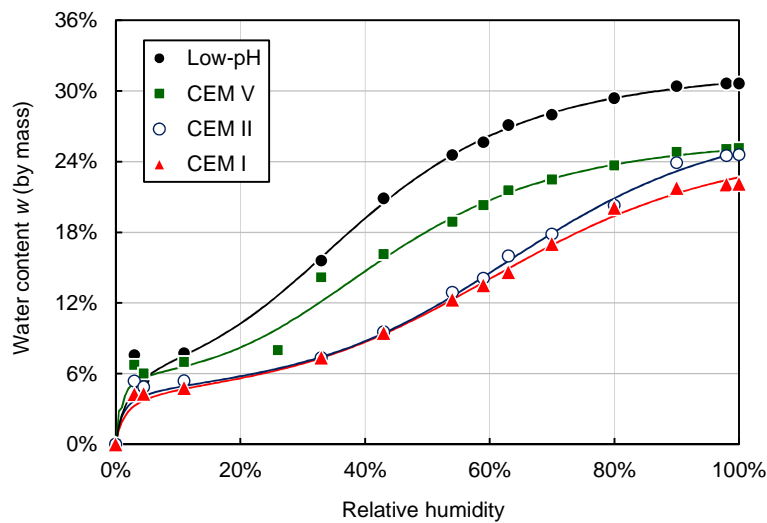


420 *Figure 6. Pore size distribution versus temperature as obtained using MIP. Each curve corresponds to the*  
 421 *mean result of 3 or 4 tests. It was not possible to obtain reliable and repeatable results for the Low-pH*  
 422 *samples kept at 80°C: these results are not presented.*

423 **4.4. Desorption isotherms**

424 The first desorption isotherm at 20°C of the four pastes are presented on Figure 7. The depicted curves  
425 are of type IV according to the classification originally proposed by Brunauer [46, 67]: one can note the  
426 monomolecular layer edification at low RH as well as the presence of a plateau near saturation (at least  
427 for CEMV and Low-pH) representative of capillary condensation within a meso-porous medium.

428



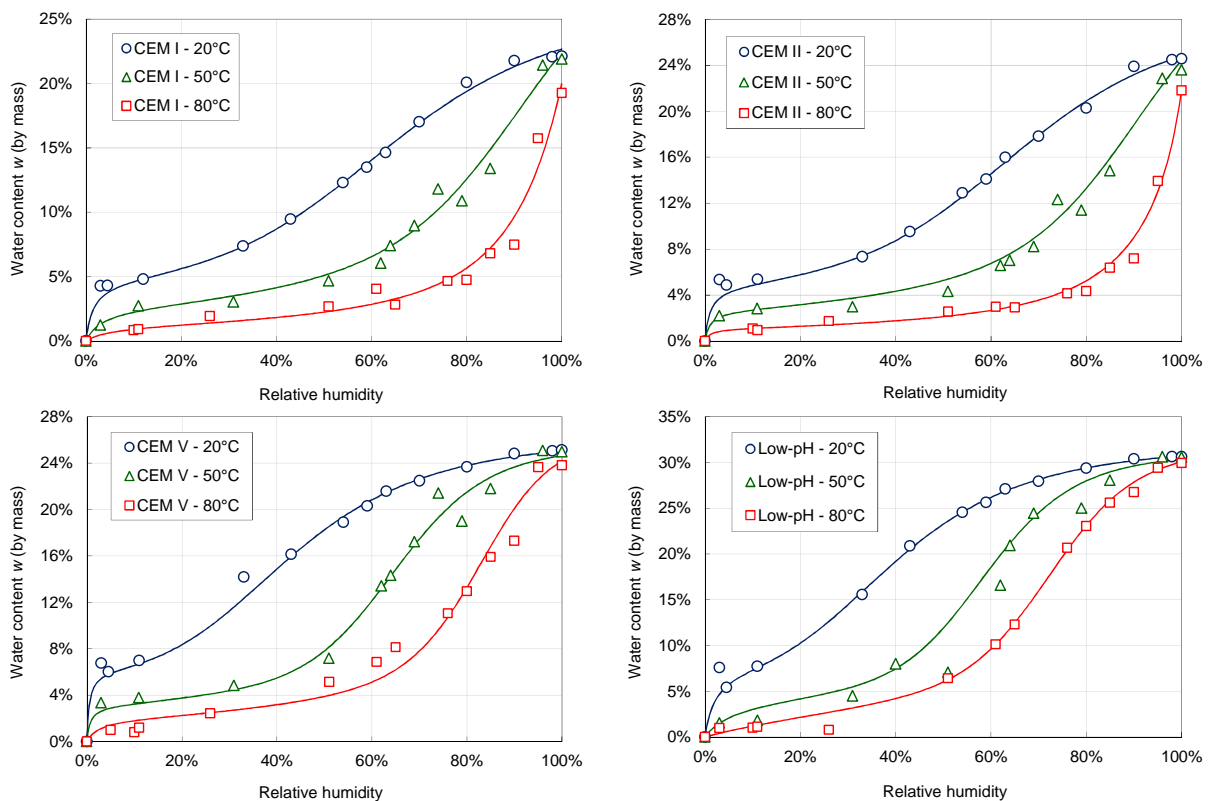
429

430 *Figure 7. First desorption isotherm at 20°C for the four pastes. Each symbol corresponds to the mean*  
431 *value of each sample set (at least three samples) whereas the solid lines (Pickett's model) are just guides*  
432 *for the eye.*

433 Similarly to the MIP results, the CEM I and CEM II pastes exhibit almost the same desorption curve  
434 despite the 25% clinker-substitution by carbonate filler. The two curves differ at high RH: the CEM II  
435 paste retains more water at saturation than the CEM I due to higher porosity. This isotherm shape is very  
436 similar to the ones obtained using ordinary cementitious materials (pastes and concretes, w/c from 0.35  
437 to 0.45) by Baroghel-Bouny [56]. The CEM V and Low-pH pastes show a different general pattern. The

438 presence of a plateau near saturation (RH=100%) is much more noticeable than for CEM I & II: the  
439 desorption isotherm slope at high RH is lower than the ones of CEM I & II (due to a refined pore size  
440 distribution). The water content at low RH (typically for monomolecular adsorption) is also higher than  
441 for CEM I & II due to higher C-S-H content.

442 The impact of temperature on the water retention curve is depicted on Figure 8. Whatever the  
443 considered paste a temperature increase induces the reduction of the water retained at equilibrium with  
444 any arbitrary RH. This effect was observed over the whole RH-range and even at RH=100% for the CEM I  
445 and CEM II pastes but was hardly observed for the CEM V and Low-pH pastes. This was attributed to the  
446 effect of ongoing hydration as detected using TGA: the resulting mass gain helped reduce the fall in  
447 water content at high RH.



448 *Figure 8. Desorption isotherm of the four hardened pastes as a function of temperature (water content).*  
449 *Each symbol corresponds to the mean value of each sample set (at least three samples) whereas the solid*  
450 *lines stand for the interpolation using Pickett's model.*

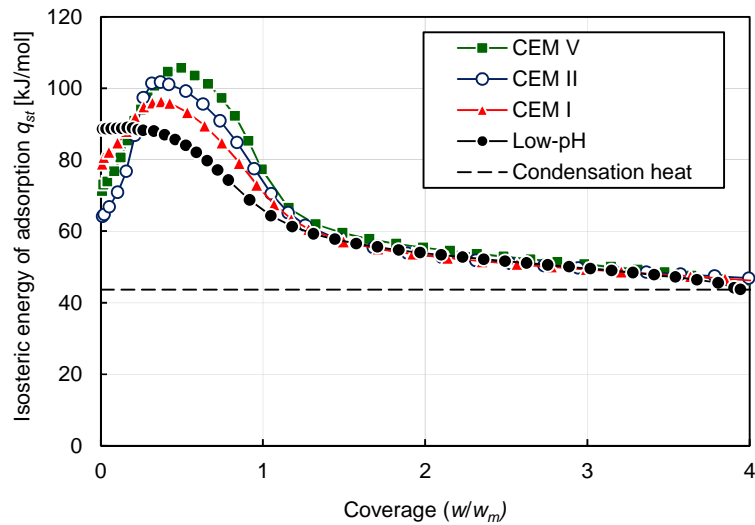
#### 451 **4.5. Isoteric energy**

452 The isosteric energy of adsorption  $q_{st}$  was assessed using eq. (1). The RH  $h$  at equilibrium with the water  
453 content  $w$  was evaluated using Pickett's model (eq. 18) and the vapor pressure  $p_v$  was calculated using  
454 Rankine's equation:

$$455 \quad p_v(w, T) = h(w, T)p_{vs}(T) = h(w, T)P_a \exp\left(\alpha - \frac{\beta}{T}\right) \quad (19)$$

456 with  $P_a=101325$  Pa;  $\alpha = 13.7$  and  $\beta = 5120$  K. The function used to interpolate  $p_{vs}(T)$  is of first  
457 importance because it appeared to influence the results obtained (the evolution remains unchanged but  
458 the values are modified). The resulting isosteric energy evolutions are plotted on Figure 9 as functions of  
459 coverage  $\frac{w}{w_m}$  (number of adsorbed layers). This presentation allows the results to be fully comparable  
460 (and not to depend on density and porosity). Apart from the Low-pH mix all the curves exhibit the same  
461 evolution:  $q_{st}$  increases at low coverage (typically between 0.0 and 0.5) from 70 kJ/mol to reach a  
462 maximal value (around 100 kJ/mol) and then continuously decreases to get close to the average water  
463 enthalpy of condensation (43.7 kJ/mol between 20 and 80°C) at high coverage. Note that the uncertainty  
464 related to the maximal isosteric evaluation process was estimated to  $\pm 10$  kJ/mol.

465



466

467 *Figure 9. Isosteric energy of adsorption  $q_{st}$  of the four considered hardened cement pastes.*

468

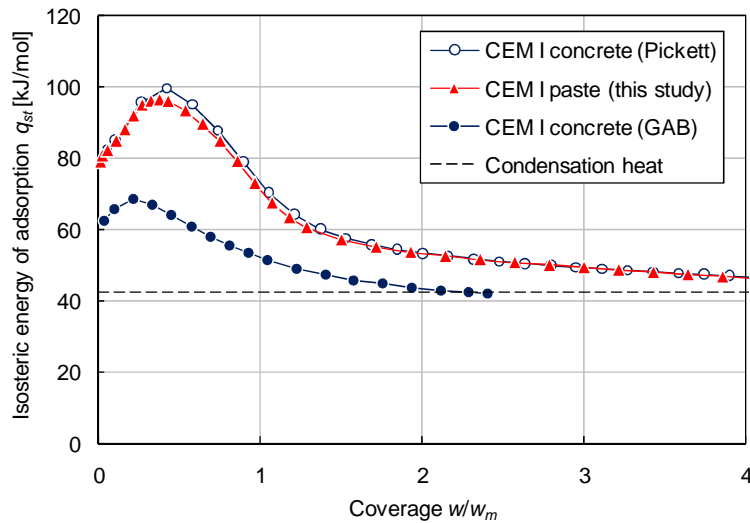
469 Most of  $q_{st}$  variations can be observed in the first layer (that is to say for  $w/w_m$  less than 1.0) which is  
 470 representative of the strong interaction between the first water layer and the hardened cement paste.

471 The  $q_{st}$  decrease (for  $w/w_m$  greater than 0.5) is representative of the decrease of the cementitious  
 472 material influence with the increase of the distance between the newly adsorbed water molecules and  
 473 substrate. The asymptotic value for high coverage (43.7 kJ/mol) corresponds to the average water  
 474 condensation energy (between 20 and 80°C): it can be considered that there is no more influence of the  
 475 cementitious material substrate and all water molecules are bonded the ones to the others (liquid state  
 476 representative of capillary condensation).

477 An increase in  $q_{st}$  in the first layer is not common: monotonic decrease is generally observed. In our case,  
 478 the maximum might just be due to the isosteric energy estimation process (use of Pickett's model rather  
 479 than another arbitrary function for instance) and to the lack (and variability) of the experimental results  
 480 in the monolayer zone (between 0 and 30% RH). Yet a maximum has already been observed for different

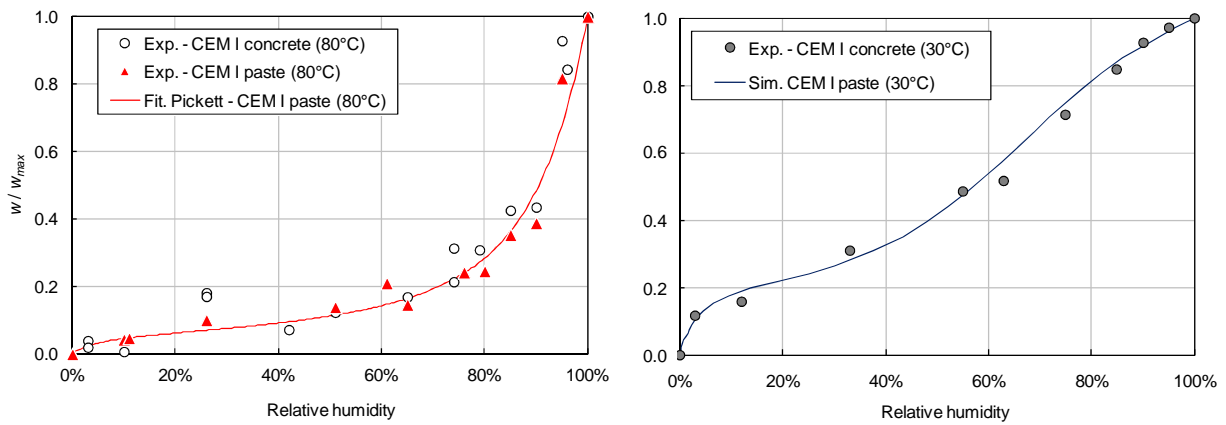
481 materials [68-76]. For hydrophobic materials such as activated carbons [70, 71]  $q_{st}$  increases from low  
482 values at low coverage (due to the lack of hydrophilic sites) up to the condensation enthalpy in relation  
483 to the formation of water clusters. For hydrophilic materials the increase is usually explained by the  
484 swelling of the dry matrix resulting in the exposure of new adsorption sites of high binding energy. When  
485 all the high energy sites are occupied water adsorption occurs on less energetic sites leading to the  $q_{st}$   
486 decrease. In the case of cementitious materials, the  $q_{st}$  increase might be due to the desaturation and  
487 the subsequent collapse of the C-S-H interlayer space [77, 78] preventing water access to high-binding  
488 energy adsorption sites within the C-S-H interlayer. This simple assumption would deserve additional  
489 experiments to be confirmed (or infirmed).

490 Figure 10 presents the comparison between the isosteric energy obtained in this study (open circles) for  
491 the CEM I paste and the corresponding concrete (filled circles) [13, 17]. It is obvious that the two  
492 evolutions do not match: the maximal value obtained for the concrete is about 66 kJ/mol whereas it  
493 reaches 100 kJ/mol for the paste. One could then conclude that there is no consistency between these  
494 two results. As a matter of fact, two different models were used to describe the desorption isotherm in  
495 both cases: GAB and Pickett models for the concrete and the paste respectively. These models were used  
496 to calculate the RH (and then the vapor pressure) at equilibrium with any arbitrary water content as  
497 needed for Clausius-Clapeyron equation, see [17] for more details. When we used Pickett's model to  
498 evaluate the concrete isosteric energy from the CEM I paste results we obtained an almost perfect  
499 match. The equation used for the description of the water retention curve (GAB or Pickett in our case)  
500 appears to be very important since it greatly influences the resulting isosteric energy  $q_{st}$ . As a  
501 consequence when handling such data, one has to be very careful and be consistent in the choice of the  
502 model used to describe the water retention curve in order to avoid erroneous results.



503  
 504 *Figure 10. Comparison between the isosteric energy evolutions obtained in this study and in a previous*  
 505 *study [13, 17].*

506  
 507 This good isosteric energy correspondence was also supported by the comparison between paste and  
 508 concrete desorption isotherm as shown in Figure 11. Figure 11 (a) presents the experimental desorption  
 509 isotherm at 80°C for the CEM I paste tested in this study and the corresponding concrete studied in [13].  
 510 To make the two isotherms comparable (porosity and density are different) the water content  $w$  was  
 511 divided by its maximal value  $w_{max}$ . The two datasets describe almost the same curve (despite the  
 512 variability). Figure 11 (b) presents the comparison between the CEM I concrete desorption isotherm  
 513 acquired at 30°C and the CEM I paste curve estimated using Clausius-Clapeyron and Pickett’s model and  
 514 the corresponding isosteric energy  $q_{st}$  (Figure 10). Once again, the comparison is very good. It is known  
 515 that for high-performance materials the presence of aggregates does not influence the water retention  
 516 curve [55, 56]: these results also show that it does not influence the isosteric energy (that is to say the  
 517 variation induced by temperature).



(a) Desorption isotherms at 80°C (CEM I paste and corresponding concrete)

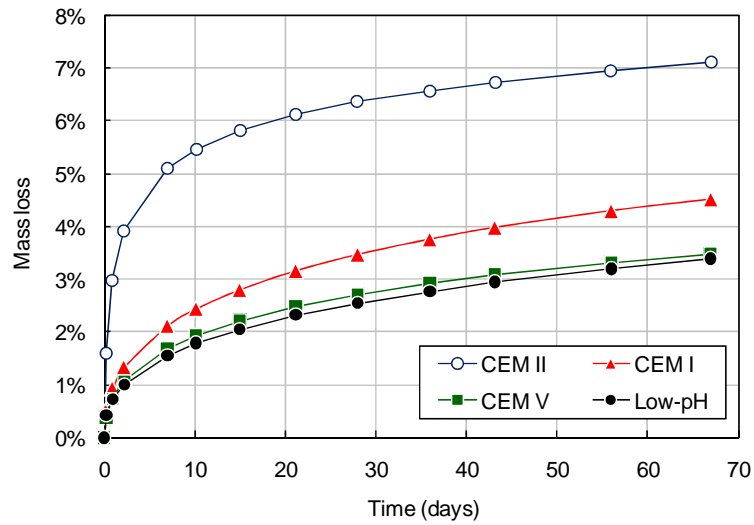
(b) Desorption isotherm at 30°C

519 *Figure 11. Comparison between the desorption isotherms of the CEM I paste tested in this study and the*  
 520 *corresponding concrete [13].*

#### 521 **4.6. Water transport**

522 Figure 12 presents the experimental mass loss evolution of the samples dried at 20°C and 54% RH (the  
 523 initial mass of the saturated specimens was taken as reference/standard to compute mass loss). The  
 524 CEM II paste exhibited the fastest mass loss (7% after 60 days) far above the CEM I (4.5% after 60 days).  
 525 Here the effect of the 25% clinker substitution by limestone filler appeared to have a significant impact  
 526 (unlike the pore-network distribution and desorption isotherm). The CEM V and Low-pH pastes showed  
 527 almost the same mass loss evolution (3.3% after 60 days).



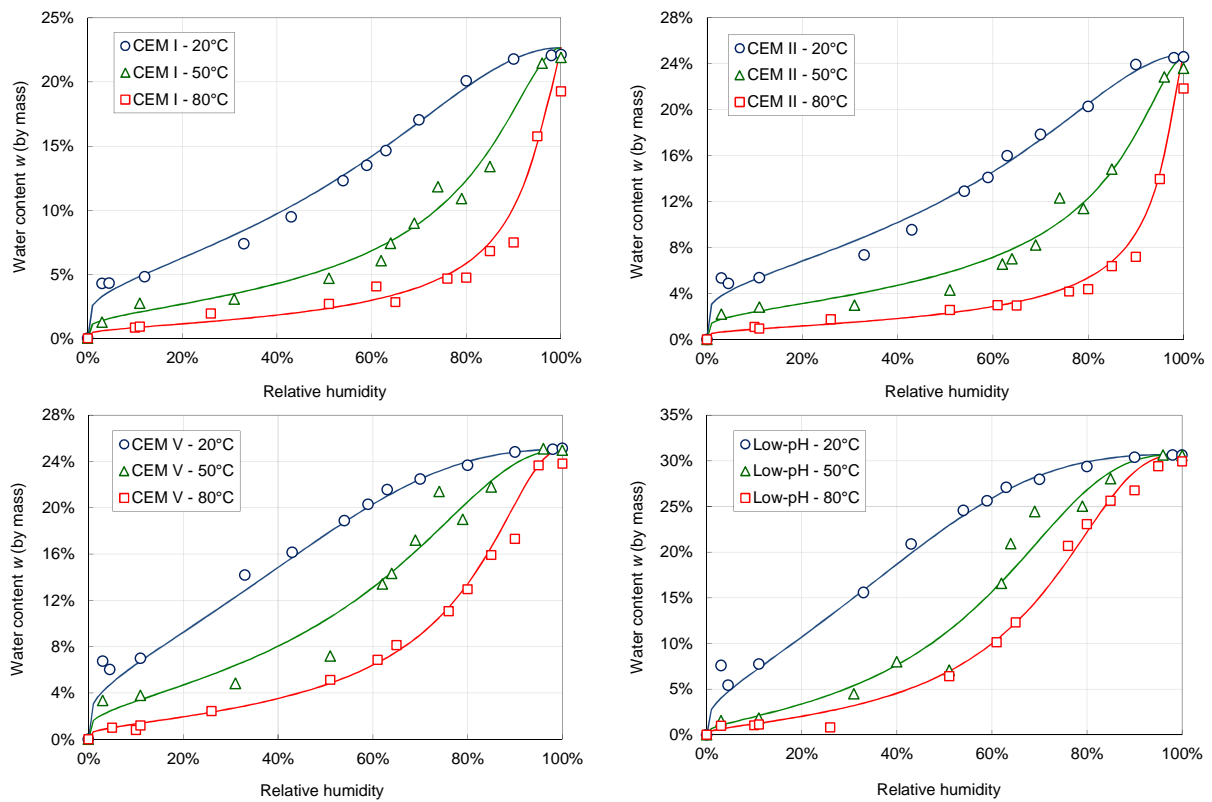


528

529 *Figure 12. Experimental mass loss of the paste samples dried at 20°C and 54% RH.*

530 The two van Genuchten's parameters  $P_0$  and  $m$  needed in eq. (8) were fitted on the experimental  
 531 desorption isotherms (Figure 13): the corresponding values are reported in Table 10. At 20°C the values  
 532 obtained are consistent with the literature [19, 22, 28]. It is noteworthy that when temperature  
 533 increases the  $m$  values remain stable whereas those of  $P_0$  decrease. The relative permeability evolutions  
 534 at 20°C are depicted on Figure 14 (a). As expected the finer the pore size distribution, the lower the  
 535 relative permeability decrease with saturation. The relative permeability evolutions can be classified in  
 536 the following order: Low-pH > CEM V > CEM I > CEM II.

537



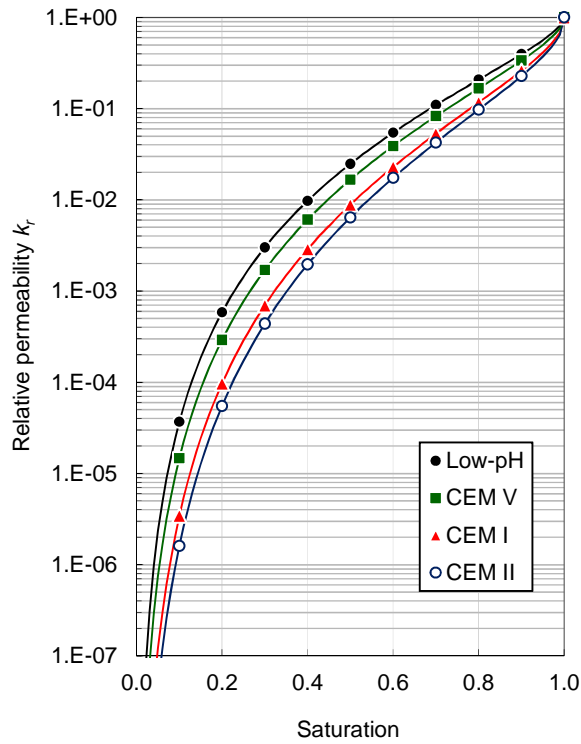
538 *Figure 13. Desorption isotherm of the four hardened pastes as a function of temperature (saturation)*  
 539 *fitted using van Genuchten equation.*

540

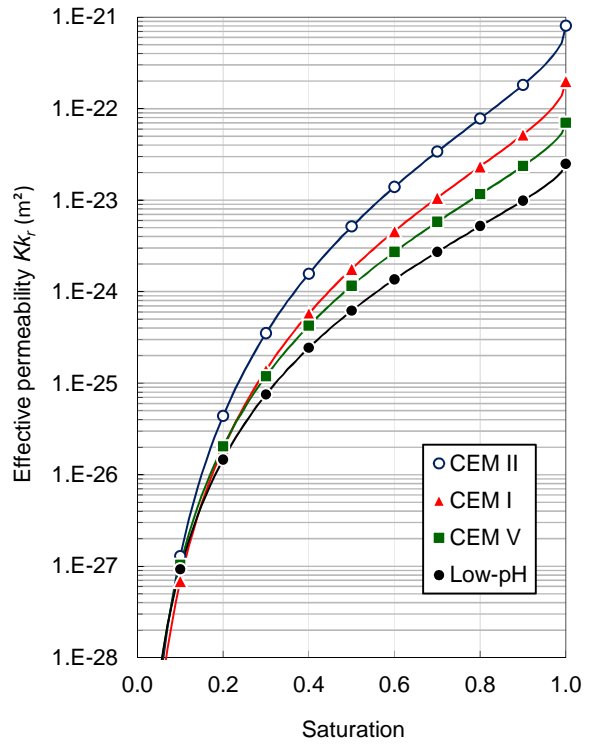
541 *Table 10. Van Genuchten parameters and permeability values.*

Paste		CEM I	CEM II	CEM V	Low-pH	Unit
20°C	$P_0$	51.4	42.5	96.9	108.7	MPa
	$m$	0.465	0.437	0.529	0.578	-
	$K$	$2.0 \times 10^{-22}$	$8.0 \times 10^{-22}$	$7.0 \times 10^{-23}$	$2.5 \times 10^{-23}$	$m^2$
50°C	$P_0$	18.9	14.7	47.1	56.8	MPa
	$m$	0.457	0.425	0.506	0.605	-
	$K$	$3.0 \times 10^{-22}$	$22.0 \times 10^{-22}$	$3.0 \times 10^{-23}$	$4.6 \times 10^{-23}$	$m^2$
80°C	$P_0$	8.1	5.2	23.5	40.3	MPa
	$m$	0.458	0.436	0.517	0.595	-
	$K$	$140.0 \times 10^{-22}$	$600.0 \times 10^{-22}$	$150.0 \times 10^{-23}$	$18.0 \times 10^{-23}$	$m^2$

542



(a) Relative permeability  $k_r$



(b) Effective permeability  $Kk_r$

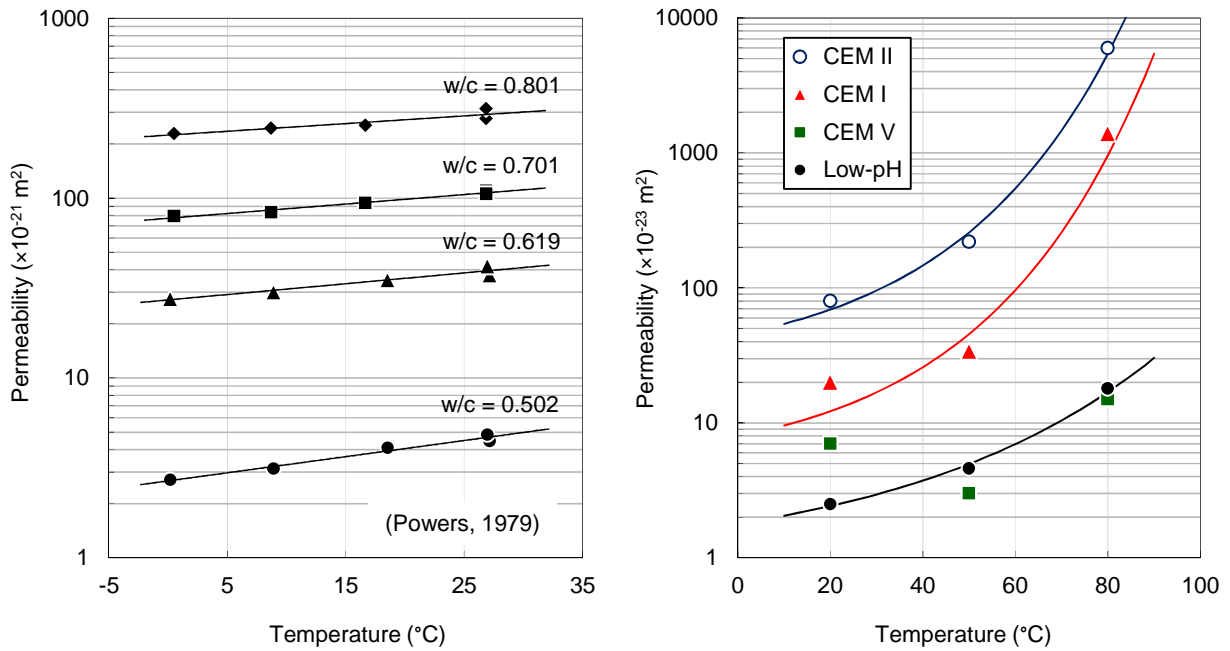
543 *Figure 14. Relative (a) and effective (b) permeability of the four hardened cement pastes at 20°C.*

544 Table 10 recapitulates the intrinsic permeability values assessed using inverse analysis. At 20°C they can  
 545 be classified in the exact inverse order obtained for the relative permeability as shown in Figure 14 (b):  
 546 CEM II > CEM I > CEM V > Low-pH. This order is consistent with the pastes pore-network fineness as well  
 547 as the C-S-H content. Figure 15 presents the permeability variations induced by temperature. Unlike the  
 548 results of Powers [5], they could not be described the classical Arrhenius law (the points were not  
 549 aligned in the log-scale plot). For fitting purposes a double exponential law (eq. 20) was alternatively  
 550 proposed:

551 
$$K(T) = K_0 \exp \left[ \exp \left( \frac{T-293.15}{T_c} \right) - 1 \right] \quad (20)$$

552 where  $K_0$  and  $T_c$  are two positive parameters, the values of which are reported in Table 11. It has to be  
 553 noted that the CEM V paste showed an unexpected and unexplained permeability decrease between 20  
 554 and 50 °C which cannot be described using eq. (18).

555



(a) Direct measurement from Powers (1979)

(b) Inverse analysis from this study

556 *Figure 15. Permeability versus temperature: (a) following Powers [5], using water permeametry between*  
 557 *0 and 30°C and (b) inverse analysis from this study.*

558 *Table 11. Parameters for the description of temperature influence on permeability (eq. 20).*

Parameter	CEM I	CEM II	CEM V	Low-pH	Unit
$K_0$	$12.2 \times 10^{-23}$	$69.1 \times 10^{-23}$	N/A	$2.4 \times 10^{-23}$	$\text{m}^2$
$T_c$	35.7	35.7	N/A	55.6	K

## 59 5. Discussion

60 The use of Clausius-Clapeyron to describe the water retention curve temperature induced modifications  
61 implicitly assumes that the cementitious material pore structure remains unchanged. This assumption  
62 was found to be acceptable for a high-performance concrete between 30 and 80°C [13]. The coarsening  
63 of the pore structure observed using MIP in this study (from 20 to 80°C) is supported by the permeability  
64 results and the unsuccessful comparison with the results of Powers [5] (Figure 15). He showed that  
65 between 0 and 30°C (temperature range within which no temperature induced modification of the pore  
66 structure was expected) the permeability variations can be fitted by a classical Arrhenius law. In our case  
67 the permeability variations are too big to be fitted by such a function. This is consistent with an increase  
68 of the transport properties associated to porosity opening. There is however other potential causes of  
69 the important permeability increase. Heating up to 80°C might have caused microcracking or increased  
70 the contribution of water transport in the gaseous phase which is not accounted for in our simplified  
71 approach. This might have resulted in overestimating the pastes permeability values at high  
72 temperature.

73 The coarsening of the pore structure observed calls into question the use of Clausius-Clapeyron and the  
74 corresponding assumption of unaltered microstructure. Indeed it is true that the pore structure coarsens  
75 when temperature increases: the error induced by our assumption also increases with temperature.  
76 Nevertheless, we believe that thermal desorption is the major mechanism at work for moderate  
77 temperatures (let us state up to 50°C). For temperatures up to 80°C, alteration of the pore structure  
78 might have a non-negligible impact on the water retention curve. Unfortunately there is nowadays no  
79 way to quantify the link the pore structure determined using MIP and the water retention curve and  
80 Clausius-Clapeyron remains the only available tool to describe the influence of temperature.  
81 Consequently it is difficult to estimate the error associated to our assumption. In a simple way one could

582 characterize the water retention curves at 20°C of samples preliminary treated at higher temperatures  
583 (from 20 to 80°C) and analyze the results to evaluate the contribution of the microstructure variation.

## 584 **6. Conclusion**

585 Temperature has a great importance for water transport in cementitious materials. This issue is of first  
586 importance for the durability assessment of reinforced concrete structures for radioactive waste  
587 management. An experimental campaign was then designed to determine the influence of temperature  
588 on cementitious materials water transport properties. Four hardened cement pastes of interest for  
589 radioactive waste management were selected. Using a simplified approach, the transport of water was  
590 described using liquid permeation only. This allowed reducing the number of properties to acquire  
591 experimentally: porosity, water retention curve and (intrinsic and relative) permeability.

592 The water retention curve was characterized using the saturated salt solution method. The unsaturated  
593 permeability was assessed using inverse analysis making use of the Mualem-van Genuchten model.  
594 Three temperatures were tested: 20, 50 and 80°C. As expected, temperature was found to have a great  
595 impact on the water retention curve: a temperature increase decreased the water content at equilibrium  
596 for all the pastes. The intrinsic permeability value significantly increased with temperature, but the data  
597 obtained do not follow Arrhenius activation law. These results constitute a valuable and consistent data  
598 set for the description of water transport in the field of radioactive waste management.

599 The temperature induced alteration of the water retention curves were described using Clausius-  
600 Clapeyron equation and the corresponding isosteric energy of adsorption was evaluated. In so doing, the  
601 microstructure was assumed not to be altered during the heating. The coarsening of the pore structure  
602 subsequent to heating was however highlighted using MIP. The water retention curve modifications

603 were then assumed to result from a combination of thermal desorption (described by Clausius-Clapeyron  
604 equation) and pore structure coarsening. The influence of the latter remains to be evaluated.

## 605 **Acknowledgements**

606 This work was financially supported by the French agency for radioactive waste management (Andra).

## 607 **7. References**

608 [1] K. Tuutti, Corrosion of steel in concrete, Swedish Cement and Concrete Research Institute, 1982, pp.  
609 468.

610 [2] B.P. Hughes, I.R.G. Lowe, J. Walker, The diffusion of water in concrete at temperatures between 50  
611 and 95°C, British Journal of Applied Physics, 17 (1966) 1545-1452.

612 [3] N.L. Hancox, The role of moisture diffusion in the drying of cement paste under the influence of  
613 temperature gradients, Journal of Physics D: Applied Physics, 1 (1968) 1769-1777.

614 [4] G.M. Glover, E. Rask, Water diffusion and microstructure of hardened cement pastes, Materials and  
615 Structures, 5 (1972) 315-322.

616 [5] T.C. Powers, The specific surface area of hydrated cement obtained from permeability data, Materials  
617 and Structures, 12 (1979) 159-168.

618 [6] J.-F. Daïan, Condensation and isothermal water transfer in cement mortar, part I - pore size  
619 distribution, equilibrium, water condensation and imbibition, Transport in Porous Media, 3 (1988) 563-  
620 589.

621 [7] S.F. Wong, T.H. Wee, S. Swaddiwudhipong, S.L. Lee, Study of water movement in concrete, Magazine  
622 of Concrete Research, 53 (2001) 205-220.

623 [8] R. Černý, J. Drchalová, P. Rovnaníková, The effects of thermal load and frost cycles on the water  
624 transport in two high-performance concretes, Cement and Concrete Research, 31 (2001) 1129-1140.

- 625 [9] M. Jooss, H.W. Reinhardt, Permeability and diffusivity of concrete as function of temperature,  
626 Cement and Concrete Research, 32 (2002) 1497-1504.
- 627 [10] J. Hundt, H. Kantelberg, Sorptionsuntersuchungen an zementstein, zementmörtel und beton (in  
628 german), Deutscher Ausschuss für Stahlbeton, Heft 297 (1978) 25-39.
- 629 [11] F. Radjy, E.J. Sellevold, K.K. Hansen, Isothermic vapor pressure-temperature data for water sorption in  
630 hardened cement paste: enthalpy, entropy and sorption isotherms at different temperatures, Report  
631 BYG-DTU R057, Technical University of Denmark (DTU), Lyngby, Denmark, 2003, pp. 58.
- 632 [12] T. Ishida, K. Maekawa, T. Kishi, Enhanced modeling of moisture equilibrium and transport in  
633 cementitious materials under arbitrary temperature and relative humidity history, Cement and Concrete  
634 Research, 37 (2007) 565-578.
- 635 [13] S. Poyet, Experimental investigation of the effect of temperature on the first desorption isotherm of  
636 concrete, Cement and Concrete Research, 39 (2009) 1052-1059.
- 637 [14] F. Brue, C.A. Davy, F. Skoczylas, N. Burlion, Effect of temperature on the water retention properties of  
638 two high-performance concretes, Cement and Concrete Research, 42 (2012) 384-396.
- 639 [15] J. Jiang, Y. Yuan, Relationship of moisture content with temperature and relative humidity in  
640 concrete, Magazine of Concrete Research, 65 (2013) 685-692.
- 641 [16] M. Wu, B. Johannesson, M. Geiker, A study of the water vapor sorption isotherms of hardened  
642 cement pastes: possible pore structure changes at low relative humidity and the impact of temperature  
643 on isotherms, Cement and Concrete Research, 56 (2014) 97-105.
- 644 [17] S. Poyet, S. Charles, Temperature dependence of the sorption isotherms of cement-based materials:  
645 heat of sorption and Clausius-Clapeyron formula, Cement and Concrete Research, 39 (2009) 1060-1067.
- 646 [18] H. Pan, J.A. Ritter, P. Balbuena, Examination of the approximations used in determining the isosteric  
647 heat of adsorption from the Clausius-Clapeyron equation, Langmuir, 14 (1998) 6323-6327.



- 648 [19] V. Baroghel-Bouny, M. Mainguy, T. Lassabatere, O. Coussy, Characterization and identification of  
649 equilibrium and transfer moisture properties for ordinary and high-performance cementitious materials,  
650 Cement and Concrete Research, 29 (1999) 1225-1238.
- 651 [20] M. Mainguy, O. Coussy, V. Baroghel-Bouny, Role of air pressure in drying of weakly permeable  
652 materials, Journal of Engineering Mechanics (ASCE), 127 (2001) 582-592.
- 653 [21] O. Coussy, Poromechanics, John Wiley & Sons Ltd2004.
- 654 [22] V. Baroghel-Bouny, Water vapour sorption experiments on hardened cementitious materials. Part II.  
655 Essential tool for assessment of transport properties and for durability prediction, Cement and Concrete  
656 Research, 37 (2007) 438-454.
- 657 [23] S. Poyet, Determination of the intrinsic permeability to water of cementitious materials: influence of  
658 the water retention curve, Cement and Concrete Composites, 35 (2013) 127-135.
- 659 [24] S. Whitaker, Simultaneous heat, mass, and momentum transfer in porous media: a theory of drying,  
660 Advances in Heat Transfer, 13 (1977) 119-203.
- 661 [25] D. Gawin, B.A. Schrefler, Thermo-hydro-mechanical analysis of partially saturated porous materials,  
662 Engineering Computations, 13 (1996) 113-143.
- 663 [26] J. Selih, A.C.M. Sousa, T.W. Bremner, Moisture transport in initially fully saturated concrete during  
664 drying, Transport in Porous Media, 24 (1996) 81-106.
- 665 [27] F. Meftah, S. Dal Pont, Staggered finite volume modeling of transport phenomena in porous  
666 materials with convective boundary conditions, Transport in Porous Media, 82 (2010) 275-298.
- 667 [28] M. Thiery, V. Baroghel-Bouny, N. Bourneton, G. Villain, C. Stéfani, Modélisation du séchage des  
668 bétons, analyse des différents modes de transfert hydrique (in French), European Journal of  
669 Environmental and Civil Engineering, 11 (2007) 541-577.

670 [29] M. Thiery, P. Belin, V. Baroghel-Bouny, M.D. Nguyen, Modeling of isothermal drying process in  
671 cementitious materials, analysis of the moisture transfer and proposal of simplified approaches, in: J.-F.  
672 Shao, N. Burlion (Eds.) 3<sup>rd</sup> international conference GeoProc, Wiley, Lille (France), 2008, pp. 571-579.

673 [30] L.A. Richards, Capillary conduction of liquids through porous mediums, *Physics*, 1 (1931) 318-333.

674 [31] B.M. Savage, D.J. Janssen, Soil physics principles validated for use in predicting unsaturated moisture  
675 movement in Portland cement concrete, *ACI Materials Journal*, 94 (1997) 63-70.

676 [32] M.T. van Genuchten, A closed-form equation for predicting the hydraulic conductivity of  
677 unsaturated soils, *Soil Science Society of America Journal*, 44 (1980) 892-898.

678 [33] Y. Mualem, A new model for predicting the hydraulic conductivity of unsaturated porous media,  
679 *Water Resources Research*, 12 (1976) 513-522.

680 [34] H. Lagrave, G. Ranc, C. Gallé, S. Durand, Durability design of heated concrete structures.  
681 Methodology and application to long-term interim storage, *Journal de Physique IV*, 136 (2006) 223-231.

682 [35] J.-P. Silvy, N. Moulin, F. Laurent, Long-term (100-300 years) interim dry storage for spent fuel:  
683 package and facilities development including safety aspects and durability assessment program, in: J.D.B.  
684 Lambert, K.K. Kadyrzhhanov (Eds.) *Safety Related Issues of Spent Nuclear Fuel Storage*, Springer, 2007, pp.  
685 181-188.

686 [36] P. de Coninck, G. Ranc, J. Iacono, J.-L. Martin, N. Moulin, K. Shirai, Y. Le Pape, E. Tronche,  
687 Contribution of Galatée on reinforced concretesStructurebBehavior for a full scales subsurface storage  
688 laboratory, in: F. Bart, C.C.D. Coumes, F. Frizon, S. Lorent (Eds.) *Proceedings of the 1<sup>st</sup> NUWCEM*  
689 *SymposiumAvignon (France)*, 2011.

690 [37] C. Cau Dit Coumes, S. Courtois, D. Nectoux, S. Leclercq, X. Bourbon, Formulating a low-alkalinity,  
691 high-resistance and low-heat concrete for radioactive waste repositories, *Cement and Concrete*  
692 *Research*, 36 (2006) 2152-2163.

693 [38] M. Codina, C. Cau-dit-Coumes, P. Le Bescop, J. Verdier, J.P. Ollivier, Design and characterization of  
694 low-heat and low-alkalinity cements, *Cement and Concrete Research*, 38 (2008) 437-448.

695 [39] R. Barneyback, S. Diamond, Expression and analysis of pore fluid from hardened psates and mortars,  
696 *Cement and Concrete Research*, 11 (1981) 279-285.

697 [40] J. Khatib, P.S. Mangat, Absorption characteristics of concrete as a function of location relative to  
698 casting position, *Cement and Concrete Research*, 25 (1995) 999-1010.

699 [41] J. Khatib, P.S. Mangat, Porosity of cement paste cured at 45°C as a function of location relative to  
700 casting position, *Cement and Concrete Research*, 25 (2003) 97-108.

701 [42] E.E. Demirci, R. Şahin, Comparison of carbonation resistance and uniformity of SCC and CC core  
702 samples, *Magazine of Concrete Research*, 2014, pp. 531-539.

703 [43] R.A. Olson, H.M. Jennings, Estimation of C-S-H content in a blended cement paste using water  
704 adsorption, *Cement and Concrete Research*, 31 (2001) 351-356.

705 [44] G. Pickett, Modification of the Brunauer-Emmett-Teller theory of multimolecular adsorption, *Journal*  
706 *of the American Chemical Society*, 67 (1945) 1958-1962.

707 [45] S. Brunauer, P.H. Emmett, E. Teller, Adsorption of gases in multimolecular layers, *Journal of the*  
708 *American Chemical Society*, 60 (1938) 309-319.

709 [46] J.B. Condon, *Surface area and porosity determinations by physisorption - Measurements & theory*,  
710 Elsevier 2006.

711 [47] P.H. Emmett, S. Brunauer, The Use of Low Temperature van der Waals Adsorption Isotherms in  
712 Determining the Surface Area of Iron Synthetic Ammonia Catalysts, *Journal of the American Chemical*  
713 *Society*, 59 (1937) 1553-1564.

714 [48] S.J. Gregg, K.S.W. Sing, *Adsorption, surface area and porosity*, 2nd ed ed., Academic Press, London,  
715 United Kingdom, 1982.

716 [49] L. Wadsö, K. Svennberg, A. Dueck, An experimentally simple method for measuring sorption  
717 isotherms, *Drying Technology*, 22 (2004) 2427-2440.

718 [50] D.S. Carr, B.L. Harris, Solutions for maintaining constant relative humidity, *Industrial and Engineering*  
719 *Chemistry*, 41 (1949) 2014-2015.

720 [51] A. Wexler, S. Hasegawa, Relative humidity-temperature relationships of some saturated salt  
721 solutions in temperature range 0°C to 50°C, *Journal of Research of the National Bureau of Standards*, 53  
722 (1954) 19-26.

723 [52] A. Scheider, Neue diagramme zur bestimmung der relativen luftfeuchtigkeit über gesättigten  
724 wasserigen salzlosungen und wasserigen schwefelsaurelosungen bei verschiedenen temperaturen (in  
725 german), *Holz als Rohstoff*, 18 (1960) 269-272.

726 [53] J.F. Young, Humidity control in the laboratory using salt solutions - a review, *Journal of Applied*  
727 *Chemistry*, 17 (1967) 241-245.

728 [54] L. Greenspan, Humidity fixed points of binary saturated aqueous solutions, *Journal of Research of*  
729 *the National Bureau of Standards - A, Physics and Chemistry*, 81A (1977) 89-96.

730 [55] V. Baroghel-Bouny, *Caractérisation des pâtes de ciment et des bétons : Méthodes, analyse,*  
731 *interprétations (in french)*, Presses du Laboratoire Central des Ponts et Chaussées, Paris, France, 1994.

732 [56] V. Baroghel-Bouny, Water vapour sorption experiments on hardened cementitious materials: Part I.  
733 Essential tool for analysis of hygral behaviour and its relation to pore structure, *Cement and Concrete*  
734 *Research*, 37 (2007) 414-437.

735 [57] C. Gallé, Effect of drying on cement-based materials pore structure as identified by mercury  
736 intrusion porosimetry. A comparative study between oven-, vacuum-, and freeze-drying, *Cement and*  
737 *Concrete Research*, 31 (2001) 1467-1477.

738 [58] M.C. Garci Juenger, H.M. Jennings, The use of nitrogen adsorption to assess the microstructure of  
739 cement paste, *Cement and Concrete Research*, 31 (2001) 883-892.

740 [59] J.J. Beaudouin, B.T. Tamtsia, Effect of drying methods on microstructural changes in hardened  
741 cement paste: an A.C. impedance spectroscopy evaluation, *Journal of Advanced Concrete Technology*, 2  
742 (2004) 113-120.

743 [60] A. Korpa, R. Trettin, The influence of different drying methods on cement paste microstructures as  
744 reflected by gas adsorption: comparison between freeze-drying, D-drying, P-drying and oven-drying,  
745 *Cement and Concrete Research*, 36 (2006) 634-649.

746 [61] P.A.M. Basheer, Permeation analysis, in: V.S. Ramachandran, J.J. Beaudouin (Eds.) *Handbook of*  
747 *analytical techniques in concrete science and technology*, Noyes Publications, Park Ridge, New Jersey,  
748 U.S.A., 2001, pp. 658-737.

749 [62] W. Klemm, Ettringite and oxyanion-substituted ettringites - their characterization and applications in  
750 the fixation of heavy metals: a synthesis of the literature, *Portland Cement Association Research and*  
751 *Development Bulletin RD116* (1998) 68p.

752 [63] Q. Zhou, F. Glasser, Kinetics and mechanism of the carbonation of ettringite, *Advances in Cement*  
753 *Research*, 12 (200) 131-136.

754 [64] Y. Aono, F. Matsushita, S. Shibata, Y. Hama, Nano-structural changes of C-S-H in hardened cement  
755 paste during drying at 50°C, *Journal of Advanced Concrete Technology*, 5 (2007) 313-323.

756 [65] X. Cong, R.J. Kirkpatrick, Effects of the temperature and relative humidity on the structure of C-S-H  
757 gel, *Cement and Concrete Research*, 25 (1995) 1237-1245.

758 [66] E. Gallucci, X. Zhang, K. Scrivener, Effect of temperature on the microstructure of calcium silicate  
759 hydrate (C-S-H), *Cement and Concrete Research*, 53 (2013) 185-195.

760 [67] K.S.W. Sing, E. D.S., R.A.W. Haul, L. Moscou, R.A. Pierotti, J. Rouquérol, T. Siemieniowska, Reporting  
761 physisorption data for gas/solid systems with special reference to the determination of surface area and  
762 porosity (Recommendations 1984), *Pure and Applied Chemistry*, 57 (1985) 603-619.

763 [68] E. Palou, A. López-Malo, A. Argaiz, Effect of temperature on the moisture sorption isotherms of  
764 some cookies and corn snacks, *Journal of Food Engineering*, 31 (1997) 85-93.

765 [69] M.M. Vivanco, O.M. Taboada, Thermodynamic behavior of fish meal during adsorption, *Drying*  
766 *Technology*, 16 (1998) 1827-1842.

767 [70] I.I. Salame, T.J. Bandosz, Experimental study of water adsorption on activated carbons, *Langmuir*, 15  
768 (1999) 587-593.

769 [71] I.I. Salame, T.J. Bandosz, Study of water adsorption on activated carbons with different degrees of  
770 surface oxidation, *Journal of Colloid and Interface Science*, 210 (1999) 367-374.

771 [72] M. Das, S. Das, Analysis of moisture sorption characteristics of fish protein myosin, *International*  
772 *Journal of Food Science and Technology*, 37 (2002) 223-227.

773 [73] N. Hamdami, J.-Y. Monteau, A. Le Bail, Transport properties of a high porosity model food at above  
774 and sub-freezing temperatures. Part 1: thermophysical properties and water activity, *Journal of Food*  
775 *Engineering*, 62 (2004) 373-383.

776 [74] S. Timoumi, F. Zagrouba, D. Mihoubi, M.M. Tlili, Experimental study and modelling of water  
777 sorption/desorption isotherms on two agricultural products: apple and carrot, *Journal de Physique IV*,  
778 122 (2004) 235-240.

779 [75] E. Quirjins, A. van Boxtel, W. van Loon, G. van Straten, Sorption isotherms, GAB parameters and  
780 isosteric heat of sorption, *Journal of the Science of Food and Agriculture*, 85 (2005) 1805-1814.

781 [76] C. Pérez-Alonso, C.I. Beristain, C. Lobato-Calleros, M.E. Rodríguez-Huezo, E.J. Vernon-Carter,  
782 Thermodynamic analysis of the sorption isotherms of pure and blended carbohydrate polymers, *Journal*  
783 *of Food Engineering*, 77 (2006) 753-760.

784 [77] R. Feldman, P. Sereda, A model for hydrated Portland cement paste as deduced from sorption-  
785 length change and mechanical properties, *Materials and Structures*, 1 (1968) 509-520.

786 [78] H.M. Jennings, Refinements to colloid model of C-S-H in cement: CM-II, Cement and Concrete

787 Research, 38 (2008) 275-289.

788